Engineering Geology 286 (2021) 106087

Contents lists available at ScienceDirect

Engineering Geology

journal homepage: www.elsevier.com/locate/enggeo

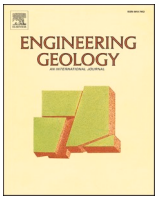

The role of interfaces in the bentonite barrier of a nuclear waste repository on gas transport

María Victoria Villar *, Beatriz Carbonell, Pedro Luis Martín, Carlos Gutiérrez-Álvarez

Centro de Investigaciones Energéticas, Medioambientales y Tecnológicas (CIEMAT), Avd. Complutense 40, 28040 Madrid, Spain

ARTICLE INFO

Keywords:
Bentonite
Gas transport
Engineered barrier
Saturation
Porosity

ABSTRACT

The FEBEX in situ test provided bentonite samples that had been submitted to the conditions of the engineered barrier of a nuclear waste repository for 18 years. These samples can be considered quite evolved from the microstructural point of view (aged, matured) when compared with samples prepared in the laboratory under shorter and more usual time scales. The barrier, composed of bentonite blocks, was hydrated with granitic groundwater under natural conditions while it was submitted to the thermal gradient generated by a heater mimicking the waste canister. Some of the samples were drilled between two bentonite blocks, therefore they were crossed along by an interface. The gas permeability of samples with and without interface was tested in the laboratory under different triaxial boundary conditions.

Samples with an interface drilled in the inner part of the barrier (i.e. closer to the heater and consequently drier) had higher gas permeability than samples of similar accessible void ratio (related to dry density and water content) with no interface, and it was necessary to apply higher confining pressures to reduce or suppress gas flow in them. Both observations point to the interface as a preferential pathway for gas flow in this kind of samples. In contrast, wetter samples drilled along interfaces of the external part of the barrier (which had very low accessible void ratio, because of the high saturation), had permeabilities similar to those corresponding to the same accessible void ratio in the reference, untreated bentonite. This would prove the healing of the interfaces between blocks as a result of full saturation. The importance of the testing boundary conditions, particularly with respect to confinement, on gas transport processes was also highlighted.

1. Introduction

Geological disposal is the preferred, internationally accepted option for wastes with high levels of radioactivity. The safety of the concept relies on a series of barriers, both engineered and natural, between the waste and the surface acting in concert to contain the wastes. Bentonites or bentonite-based materials have frequently been proposed to construct the engineered barrier around the waste container (buffer) because of their high retention capacity, high swelling ability and low permeability.

The heat released by the waste will induce a thermal gradient through the bentonite barrier, while groundwater will tend to flow into it. As a consequence, coupled thermal, hydraulic, mechanical and geochemical processes will take place during the transient period of the repository life. In advance stages of the repository gas will be generated by several mechanisms, such as the anaerobic corrosion of metals, the microbial degradation of organic wastes and the radiolysis of water, which generate hydrogen, oxygen, methane and carbon dioxide. The gas generated can dissolve in the pore water according to Henry's law and move away with it, but if the volume of gas generated is too large, a separate gas phase would exist in the bentonite barrier (e.g. Ortiz et al., 2002). The transport of this gas phase would involve both visco-capillary two-phase flow under low pressure (without significant deformation of the pore space) and microscopic pathway dilation, depending on the degree of saturation of the bentonite, i.e. on the gas accessible void ratio (Olivella and Alonso, 2008; Sellin and Leupin, 2013; Villar et al., 2013; Graham et al., 2016). If the generation rates are higher than the rate by which gas is transported away within the repository, the gas pressure could rise and build up, but gas migration would not occur unless the applied gas pressure exceeded the total stress experienced by the clay (resulting from the sum of the water pressure and the swelling pressure), i.e. until the *breakthrough* value was reached (Horseman et al., 1999; Harrington and Horseman, 2003). As a result, a mechanical interaction between the gas and clay will begin, leading to

* Corresponding author.
E-mail address: mv.villar@ciemat.es (M.V. Villar).

https://doi.org/10.1016/j.enggeo.2021.106087
Received 21 August 2020; Received in revised form 20 January 2021; Accepted 4 March 2021
Available online 9 March 2021

the generation of gas pathways, which might affect the barrier properties and drive contaminated water into the geosphere. Thus, the knowledge of the movement of gases through the repository structure is required to determine the magnitude of these effects and to accommodate them in the repository design and safety calculations.

In the context of studies related to the geological disposal of radioactive waste, and with a focus on the engineered barrier performance, the FEBEX in situ test was the first real scale test of a horizontal disposal system for high-level radioactive waste, performed under natural conditions in crystalline rock (ENRESA 2006). A gallery of 2.3 m in diameter was excavated through the granite at the Grimsel Test Site (Switzerland) and two heaters, that simulated the thermal effect of the wastes, were placed concentrically, surrounded by a barrier of highly-compacted bentonite blocks. The external surface temperature of the heaters was 100 °C and the bentonite was slowly hydrated by the granitic groundwater. After 5 years of operation, half of the installation was dismantled, and the other half continued in operation with just one heater under the configuration shown in Fig. 1. In 2015, after 18 years operation, the FEBEX Dismantling Project (FEBEX-DP) undertook the dismantling of the remaining half of the experiment (García-Siñeriz et al., 2016).

The bentonite engineered barrier of the FEBEX in situ test was composed of compacted blocks among which there were interfaces (Fig. 2). The blocks were manufactured in the shape of 12-cm thick circular crown sectors and arranged in vertical slices consisting of concentric rings. The blocks were obtained by uniaxial compaction of the FEBEX clay with its hygroscopic water content applying pressures of between 40 and 45 MPa, what caused dry densities of 1.69–1.70 g/cm^3. The initial dry density of the blocks was selected by taking into account the probable volume of the construction gaps and the need to have a barrier with an average dry density of 1.60 g/cm^3 (ENRESA 2006). The initial aspect of some of these construction gaps can be seen on the left-hand side of Fig. 2, whereas their appearance upon dismantling after 18 years operation is shown on the right-hand side. The hydration and swelling of the bentonite caused the closing and sealing of all the gaps, both those among blocks of the same slice and the gaps between adjacent bentonite slices that cannot be seen in this Figure. There was no effect of the vertical gaps between bentonite slices on the water content and dry density distribution, which proves that they were not preferential water pathways (Villar et al., 2016, 2020a). The same had already been observed during the partial dismantling, after five years of operation (Villar et al., 2005). Fig. 1 shows the water content isolines of the barrier drawn from on-site measurements performed during dismantling in 2015. The water content was higher than the initial one in all locations, but decreased from the granite towards the heater, whereas the dry density increased in the same sense (Villar et al., 2016, 2020a).

During dismantling numerous bentonite samples were taken and sent to different laboratories for analysis. Some of the samples were obtained by drilling the bentonite surface exposed when the previous bentonite slice was removed. The gas permeability of some of these core samples was measured with the aim of checking:

- the influence on gas permeability of the physical state of the samples in terms of water content and dry density and consequently of degree of saturation,
- the effect of the boundary conditions on gas permeability, namely gas injection pressure and confining pressure,
- the change of gas transport properties with respect to the untretated, reference FEBEX bentonite and
- the role of interfaces on gas transport.

To accomplish the last aim, the samples were drilled both in the middle of blocks and along the interface between two blocks, as indicated in Fig. 2. Fig. 1 shows the sampling sections from which the samples tested in this investigation were taken.

To the authors' knowledge, the research reported in this paper is the first systematic study on the gas transport properties of bentonite samples submitted to repository-like conditions for a long period of time, consequently of matured, aged bentonite. It is also the first experimental investigation about the role on gas transport of interfaces between bentonite blocks of an engineered barrier.

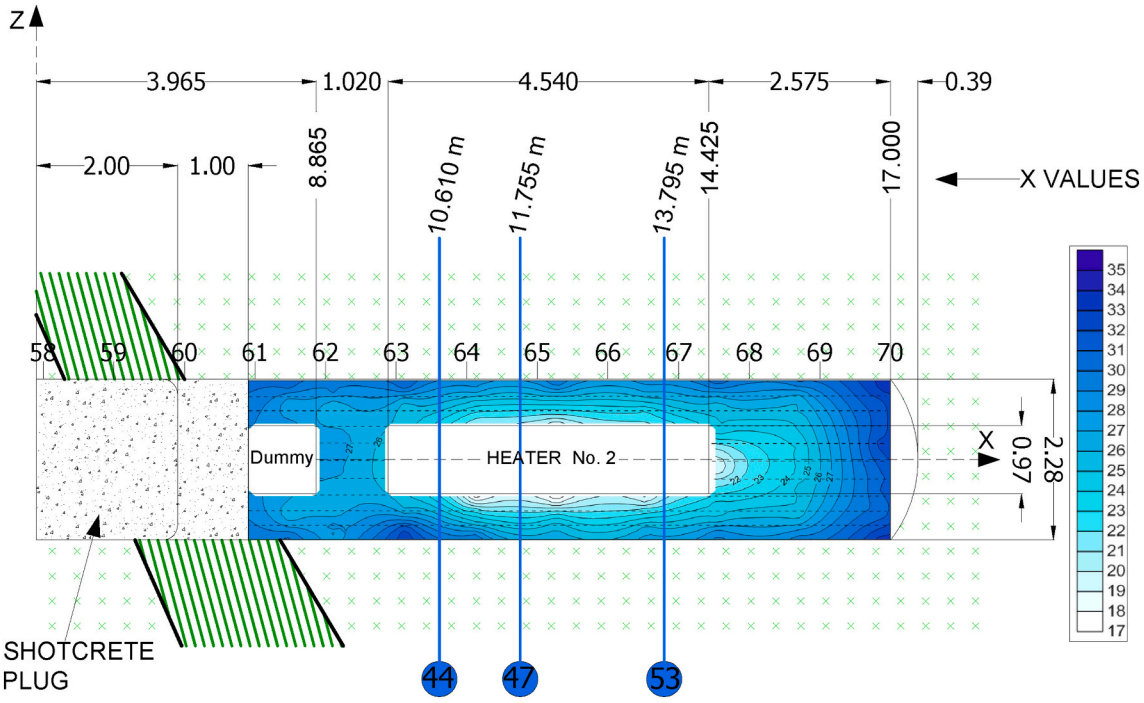

Fig. 1. Layout of the FEBEX in situ test during the second operational phase and location of the sampling sections from which the samples for the gas transport tests were taken (distances in m, modified from Bárcena and García-Siñeriz, 2015). The contour lines correspond to the water content of the bentonite determined upon dismantling (Villar et al., 2016).

Fig. 2. Appearance of the bentonite barrier around Heater #2 during installation in 1997 and during dismantling in 2015 (the block contours were difficult to tell apart and have been indicated by discontinuous lines.) Examples of the location of samples drilled for gas testing are marked with circles.

2. Background: gas transport studies in FEBEX bentonite

The research on the gas transport properties of FEBEX bentonite started back in the 90s, when the gas permeability of samples compacted to different dry densities and water contents was measured in a falling-head permeameter (described below in section 3.3.1), using very low injection pressures (Villar and Lloret, 2001; Villar, 2002). Gas permeability was found to depend on the accessible void ratio, which expresses the ratio between gas accessible volume (not blocked by water) and particle volume. It is computed as e (1-S_r), with e being the void ratio and S_r the degree of saturation. It was also found that the intrinsic permeability deduced from gas flow was considerably higher than that deduced from water flow, which was because of the microstructural changes that take place during saturation, namely the reduction in average pore size. Because of the equipment limitations, it was not possible to measure the gas permeability of samples with high degrees of saturation. New setups were developed in the framework of the European FORGE project (https://www.bgs.ac.uk/forge/), which allowed to measure the permeability of samples with degrees of saturation up to 97% and test the effect of confining pressure and gas injection and backpressures on the gas permeability value. In these tests, the applied pressure gradient directly controlled the resulting gas flow rate, attesting conventional visco-capillary flow. The new results also allowed to confirm the potential relation between accessible void ratio and gas permeability, with exponents between 3 and 4. Furthermore, it was checked that the Klinkenberg effect was not significant for this material in the range of pressure tested (Villar et al., 2013; Gutiérrez-Rodrigo, 2018).

The tests mentioned in the previous paragraph were all performed in triaxial cells. But during the FORGE project, tests were also performed on samples fully saturated inside stainless steel cylindrical cells, where the overall volume of the bentonite could not change during the tests. Those tests were designed to determine the gas breakthrough pressure and additionally estimate a permeability value once breakthrough occurred (Villar et al., 2013; Gutiérrez-Rodrigo et al., 2015, 2021; Gutiérrez-Rodrigo, 2018). These permeability values were computed assuming two-phase flow as gas transport mechanism for lack of a better approximation. The gas breakthrough pressure values in saturated bentonite increased clearly with dry density, and they were always higher than the swelling pressure of the bentonite. The permeabilities computed after breakthrough seemed to be independent of the dry density (Gutiérrez-Rodrigo et al., 2021).

The tests performed in the triaxial cells and in the stainless steel cells mentioned above were designed to measure the bentonite gas permeability and the gas breakthrough pressure, respectively. The combination of both types of results allowed to conclude that in compacted bentonite two-phase flow can take place for degrees of saturation lower than about 97%, whereas, for higher degrees of saturation, pathway dilation could be the predominant mechanism after a given breakthrough pressure was reached. The stability of the pathways would depend on the degree of saturation and dry density of the samples. For partially saturated bentonite, the gas pathways seemed to be stable, since for a given pressure gradient there was a stable flow. Nevertheless, the drop in effective gas permeability when approaching full saturation is that of several orders of magnitude (Villar et al., 2013; Gutiérrez-Rodrigo et al., 2015), indicating an important restriction of the gas flow inside the bentonite. In almost completely saturated samples of bentonite, in which it was necessary to apply a high pressure to induce flow (breakthrough pressure), when the pressure gradient dropped below a given value (residual pressure), flow stopped, which was interpreted as the closing of the pathways.

In the gas breakthrough tests, the role of an interface along the cylindrical specimen was tested. To this aim, the cylindrical specimen obtained by uniaxial compaction was longitudinally cut and the two halves obtained were put together in the stainless steel cell and then saturated prior to breakthrough testing. The results indicated that a sealed interface along a saturated bentonite specimen had no effect on the breakthrough pressure values (Gutiérrez-Rodrigo et al., 2021).

The specimens used to perform the tests summarised above were obtained either by uniaxial compaction of the granulated bentonite mixed with different quantities of deionised water (tests in triaxial cells), or by compaction of the bentonite with its hygroscopic water content that was subsequently saturated inside the testing cell (tests in isochoric stainless steel cells). In the latter case the samples were saturated for periods of time that spanned from 2 to 28 months. In addition to these kinds of samples, specimens coming from the final dismantling of the FEBEX in situ test were also tested for gas permeability in the triaxial cells. These samples had been subjected to repository-like conditions for 18 years and were consequently quite “mature” in terms of evolution of the microstructure, which is something that cannot be reached in laboratory experiments. They were overall highly saturated, except for those taken closer to the heater that simulated the waste container. Namely, samples with initial degrees of saturation between 79 and 100% were tested. The results obtained were reported in Villar et al.

(2018a) and part of them published in Carbonell et al. (2019). The whole set of results is summarised here, including those obtained in samples with interface.

3. Material and methods

3.1. Material: the FEBEX bentonite

The material used to construct the clay buffer of the FEBEX in situ test was the FEBEX bentonite, extracted from the Cortijo de Archidona deposit (Almería, Spain). At the factory, the clay was disaggregated and gently dried to a water content of around 14%, all the material of particle size greater than 5 mm being rejected. The processed material was used for fabrication of the blocks for the large-scale test and for the laboratory tests performed for the characterization of the clay. The physico-chemical properties of the FEBEX bentonite, as well as its most relevant thermo-hydro-mechanical and geochemical characteristics were reported in ENRESA (2006) and updated in e.g. Villar (2017) and are summarised below.

The smectite content of the FEBEX bentonite is above 90 wt%. The smectitic phases are actually made up of a montmorillonite-illite mixed layer, with 10–15 wt% of illite layers. Besides, the bentonite contains variable quantities of quartz, plagioclase, K-felspar, calcite, and cristobalite-trydimite. The cation exchange capacity is 98 ± 2 meq/100 g, the main exchangeable cations being calcium (35 ± 2 meq/100 g), magnesium (31 ± 3 meq/100 g) and sodium (27 ± 1 meq/100 g). The predominant soluble ions are chloride, sulphate, bicarbonate and sodium.

The liquid limit of the bentonite is 102 ± 4%, the plastic limit 53 ± 3%, the density of the solid particles 2.70 ± 0.04 g/cm^3, and 67 ± 3% of particles are smaller than 2 μm. The hygroscopic water content in equilibrium with the laboratory atmosphere (relative humidity 50 ± 10%, temperature 21 ± 3 °C) is 13.7 ± 1.3%. The external specific surface area is 32 ± 3 m^2/g and the total specific surface area is about 725 ± 47 m^2/g.

The saturated hydraulic conductivity of compacted samples of the FEBEX reference bentonite is exponentially related to their dry density. The empirical relationship between intrinsic permeability (k_{iw}, m/s) and dry density (ρ_d, g/cm^3) shown in Eq. 1 was obtained for samples compacted to dry densities above 1.47 g/cm^3 and permeated with deionised water at room temperature (Villar, 2002). According to this relationship, for a dry density of 1.6 g/cm^3 the intrinsic permeability of the bentonite is about 5·10^{-21} m^2.

$$log\ k_{iw} = -2.96\ \rho_d - 15.57 \quad (1)$$

The swelling pressure (P_s, MPa) of compacted samples is also exponentially related to the bentonite dry density, according to the empirical expression in Eq. 2 (Villar, 2002), which indicates that when the bentonite at dry density of 1.6 g/cm^3 is saturated under constant volume with deionised water at room temperature, the swelling pressure has a value of about 6 MPa:

$$ln\ P_s = 6.77\ \rho_d - 9.07 \quad (2)$$

As mentioned in section 2, the gas effective permeability of samples of FEBEX bentonite compacted to different dry densities with various water contents was measured under confining pressures of 0.6 and 1.0 MPa (Villar, 2002; Villar et al., 2013). The gas permeability values obtained were related to the accessible void ratio through

$$k_{ig} \cdot k_{rg} = 1.25 \cdot 10^{-12}\ (e(1 - S_r))^{3.22} \quad (3)$$

3.2. Sample preparation

The samples used were obtained by drilling the bentonite barrier of the FEBEX in situ test at the Grimsel Test Site during dismantling (named hereafter FEBEX-DP samples). Half of the samples were drilled in the middle of blocks and the other half at the contact between two blocks, so that to have an interface along the core. The name of the samples was given as BC-SS-n, where BC stands for "bentonite core", SS indicates the section from which the sample was drilled (S44, S47, S53, according to Fig. 1) and n is a consecutive number.

To prepare the samples in the laboratory, the core diameter was fit to that of the testing cells (36 or 50 mm) by using a cutting ring and a knife and sand paper in some cases. The cylindrical surface of the samples was smoothed and the parallelism of the cylinder's ends was ensured. The resulting specimens were between 2.4 and 5 cm in height and 10–20 cm^2 in surface area. In some cases the interface along the core became distinct only after preparing the specimen (Fig. 3). To determine the initial water content and dry density of the samples (and in some cases the pore size distribution), a spare fragment resulting from the sample preparation was used. The characteristics of the samples have been included in Table SM1 (in Supplementary Material, available online). The initial water contents determined in these core samples were similar, or slightly higher, than those determined in adjacent blocks, which were used to draw the isolines plotted in Fig. 1 (also included in Table SM1 and compared in Fig. SM1). The process of trimming could have caused certain external drying of the samples, as discussed below in section 4.5.

Filter paper and porous stones were placed on top and bottom of the samples. The assemblage thus prepared was laterally wrapped in double latex membranes or in EPDM (ethylene propylene diene monomer) rubber over a latex membrane. Other samples were wrapped in duct tape and finally in an EPDM rubber membrane. Vacuum grease was applied between membranes in order to prevent the loss of gas. These assemblages were placed in triaxial cells.

3.3. Experimental setups

The same sample was tested consecutively in two different setups without removing it from the triaxial cell. The first setup, which worked as a low-pressure, falling-head permeameter, had been used in the investigations with FEBEX bentonite initially reported in Villar and Lloret (2001) and Villar (2002), where the setup was described in detail. Results obtained in this setup for the reference, untreated bentonite were used to assess the changes in the gas transport properties of the FEBEX-DP samples (see section 4.4). The second setup was a high-pressure equipment that could either work as a falling-head (unsteady-state) or as a constant-head (steady-state) permeameter. Under both configurations a variety of boundary conditions was allowed (Villar et al., 2018a; Carbonell et al., 2019).

A total of 19 core samples were tested, eight of which were crossed by an interface. Only four of them were not initially tested in the low-pressure equipment.

3.3.1. Low-pressure equipment (LP)

Once the triaxial cell was filled with water, a confining pressure high enough to ensure perfect adherence of the membranes to the surface of the sample was applied to the chamber of the triaxial cell. The inlet at the lower part of the sample was connected to an airtight tank of known volume, in which nitrogen gas was injected at a pressure slightly higher than atmospheric. The tank was instrumented with a pressure sensor connected to a data acquisition system which recorded the pressure of the fluid contained inside. The inlet at the upper end of the sample was left open to the atmosphere. The test consisted in allowing the gas in the tank to go out to the atmosphere through the specimen, while the decrease in pressure in the tank was measured as a function of time. A schematic design of this setup is shown in Fig. SM2.

The effective permeability to gas ($k_{ig} \cdot k_{rg}$ [m^2], with k_{ig} being the intrinsic permeability measured with gas [m^2] and k_{rg} the relative permeability to gas) was calculated in accordance with the following equation (Yoshimi and Osterberg, 1963):

Fig. 3. Initial appearance of sample BC-53-4.

$$k_{ig}\cdot k_{rg} = 2.30 \times \frac{V\cdot L\cdot \mu_g}{A \times \left(P_{atm} + \frac{P_0}{4}\right)} \times \frac{log_{10}\left(\frac{P(t)}{P_0}\right)}{t - t_0} \quad (4)$$

where V is the volume of the tank (m^3), L is the length of the sample (m), A is the surface area of the sample (m^2), μ_g is the dynamic viscosity of nitrogen under the test conditions ($1.78\cdot10^{-5}$ Pa·s), P_{atm} is atmospheric pressure (Pa), P_0 is the excess pressure over atmospheric pressure in time t_0 (s) and $P(t)$ is the excess over atmospheric pressure (Pa) in the tank at time t (s). This equation was developed in a way analogous to that used for the expression of permeability to water using a falling head permeameter, with the air continuity equation being applied through consideration of compressibility (Lloret, 1982).

The volume of the spherical tank used was $2.21\cdot10^{-2}$ m^3 and the gas used for the tests was nitrogen, for which a density of 1.12 kg/m^3 was taken. The tests were performed at room temperature (22.6 ± 1.3 °C). Prior to every new permeability test, the airtightness of the system was checked.

Taking into account the cited values for the density and the viscosity of nitrogen, the following relation between permeability to gas (k_g, m/s) and the effective permeability in Eq. 4 is obtained:

$$k_g = \frac{\rho_g\cdot g}{\mu_g} \times k_{ig} \times k_{rg} = 6.2\cdot10^5 \times k_{ig} \times k_{rg} \quad (5)$$

The triaxial cell was initially pressurised to 0.6 MPa. This confining pressure was chosen because it is well below the apparent preconsolidation stress of the samples and consequently would not cause any significant sample deformation (swelling during the tests was not expected because no additional water was provided to the samples). The pressure of the tank on test initiation was fixed to values close to 103 kPa (relative pressure). The test continued until the pressure decrease rate allowed to compute a constant permeability value or until the pressure tank was emptied. In some of the samples no flow occurred under these pressure conditions, but if flow took place, the confining pressure was increased to 1 MPa, and the test was repeated, previously increasing again the gas tank pressure. Afterwards, the cell with the sample was moved to the high-pressure equipment.

3.3.2. *High-pressure equipment (HP)*

Two different configurations of the high-pressure gas permeability setup were used for these tests, which were performed in the same samples previously tested in the low pressure equipment described above (Villar et al., 2018a). The first tests were performed in a setup in which a small gas cylinder was connected to the upper end of the sample, the pressure in it was initially fixed and allowed to decrease as flow took place through the sample, following the working principle of an unsteady-state permeameter (HP-US). Only three samples were tested under this configuration. Afterwards the setup was modified in order to improve the accuracy of the results of the tests, and flowmeters were installed to measure gas outflow. Under this configuration the tests were performed by keeping constant confining and injection pressures and atmospheric backpressure, i.e. following the working principle of a steady-state permeameter (HP-S).

The general testing protocol followed approximately these phases:

- Phase 1: the tests started under confining pressure of 0.6 or 1 MPa (depending on the last confining pressure applied in the LP setup), injection pressure of 100 kPa and atmospheric backpressure. If there was no flow or it was very low, the injection pressure was increased in 100-kPa steps to cause larger flow.
- Phase 2: Once the flow was sufficiently high to be measured accurately or the difference between confining and injection pressures was lower than 200 kPa (to ensure that gas flow did not take place between the membrane and the sample external surface), the confining pressure was progressively increased until gas could not flow through the sample.
- Phase 3: Finally, the confining pressure was stepwise decreased, keeping the injection pressure constant.

The particular pressure values reached in each of these phases depended on the characteristics of the samples. In those with high permeability, Phase 1 was very short (the injection pressure did not have to be increased because flow was initially high) and the confining pressure in Phase 2 had to be increased to very high values to stop flow. In contrast, some samples with very low permeability could only be submitted to Phase 1, because flow was too low to decrease it even further by increasing the confining pressure.

The duration of each step was nominally fixed to 24 h, although when flow was high it had to be shortened to avoid unnecessary drying of the samples or exhausting of the pressure vessels.

3.3.2.1. High-pressure, unsteady-state (HP-US). The general setup consisted of two stainless steel pressure cylinders connected to the inlets of

the triaxial cell and equipped with pressure sensors: an inlet transducer GE UNIK 5000 (350 bar-a, 0.04% FS BSL) and an outlet transmitter DRUCK PTX 1400 (100 bar-sg, 0.25% BSL max). Vacuum was applied to the downstream cylinder (the one connected to the bottom of the sample) and the other one was pressurised with nitrogen gas to 200 kPa. If no changes in pressure were recorded for 24 h, the injection pressure was increased by 100 or 200 kPa. The process was repeated until gas started to flow through the sample, causing a decrease of pressure in the upstream cylinder and an increase in the downstream one. The confining pressure was applied to the water in the triaxial cell with a pressure bladder accumulator or a pressure/volume piston controller. A schematic design of the setup is shown in Fig. 4.

Instantaneous gas flow rates under the imposed pressure gradient, entering in or coming out from the sample, could be calculated from the volume of the upstream/downstream cylinders and the instantaneous rate of pressure change (Loosveldt et al., 2002), avoiding the need for a flow-rate measuring device. Hence, the mean volume flow rate Q_m, where the subscript 'm' refers to reference conditions of T and P under which the mass flow was measured, was calculated as:

$$Q_m = V_v \times \left(\frac{\Delta\rho}{\rho}\right) \times \frac{1}{\Delta t} \tag{6}$$

where V_v is the volume of the cylinder (150 or 300 cm^3), $\Delta\rho/\rho$ is the relative change in gas density, and Δt is the time interval in which the change in gas density took place.

Considering that the tests were isothermal, the following relation can be obtained (see Gutiérrez-Rodrigo et al., 2015; Gutiérrez-Rodrigo, 2018):

$$Q_m = V_v \times \left(\frac{\Delta P}{P_{av}}\right) \times \frac{1}{\Delta t} \tag{7}$$

where V_v is the volume of the cylinder, ΔP is the pressure change and P_{av} is the average pressure (upstream or downstream) in the cylinder (inlet or outlet) during the time interval considered (Δt).

To compute the effective permeability ($k_{ig}{\cdot}k_{rg}$, m^2) the gas inflow or outflow can be used, applying the following equation for incompressible media with compressible pore fluids (Scheidegger, 1974):

$$k_{ig}{\cdot}k_{rg} = \frac{Q_m \times \mu_g \times L \times 2P_m}{A \times \left(P_{up}^2 - P_{dw}^2\right)} \tag{8}$$

where Q_m is the mean volume flow obtained applying Eq. 7, A, μ_g and L are the same as in previous equations and P_{up} and P_{dw} are the upstream and downstream pressures (kPa) applied at the top (inlet) and the bottom (outlet), respectively, of the sample. In this kind of tests the measurement pressure P_m and the average pressure of the interval P_{av} are the same.

The accuracy of this analysis depends on these assumptions: 1) the gas compressibility did not affect the volumetric flow (gas behaved as an ideal gas), and 2) a quasi-steady mass-flow state was established, i.e. the quantity of gas exiting the high pressure cylinder was approximately equal to that entering the low pressure cylinder, without accumulation of gas mass inside the sample over the time period of interest.

3.3.2.2. High-pressure, steady-state (HP-S). In this setup the injection pressure could be independently varied and maintained constant during the period of time necessary to get steady flow, while the backpressure remained atmospheric and the outflow was measured. Outflow gas rates, upstream and downstream pressure, confining pressure and temperature were monitored online. The equipment was described in detail in Villar et al. (2018a) and Carbonell et al. (2019) and is shown in Fig. SM3.

The same gas injection lines as in the HP-US configuration were used, which allowed to apply injection pressures of up to 18 MPa. The outlet of the cell connected to the bottom of the sample was open to atmosphere, with a series of different range HITECH gas mass flowmeters (0.04–2, 0.2–10, and 2–100 STP cm^3/min) measuring the gas outflow, the value used to compute permeability being the one measured by the flowmeter working in the proper range. To apply the confining pressure the same devices as in the HP-US equipment were used.

To compute the apparent (effective) permeability, the gas outflow measured was used in Eq. 8. In this kind of test, Q_m is the mean volume flow rate measured by the appropriate flowmeter, P_m is the standard atmospheric pressure (101.325 kPa) due to the STP conditions of the gas

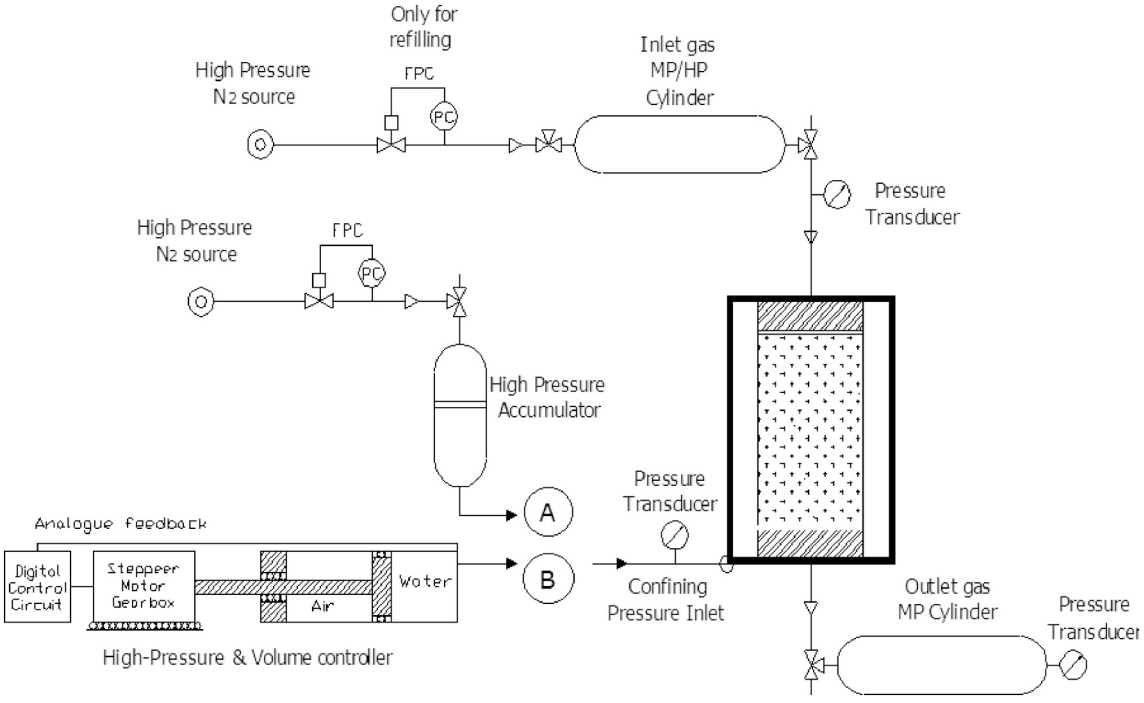

Fig. 4. Schematic diagram of the setup for the high-pressure unsteady equipment (HP-US) with the two options for applying confining pressure: A) HP accumulator; B) P/V controller.

mass flowmeters and ($P^2_{up} - P^2_{dw}$) is the difference between the gas injection pressure and the backpressure (actual atmospheric pressure in this setup).

3.4. Final determinations

At the end of the tests, the bentonite specimens were measured and weighed and the water content and dry density at three different levels (two, if they were too short) along the cylindrical specimens were determined. To determine the dry mass of the samples they were oven-dried at 110 °C for 48 h, and to compute the dry density, the volume of the same specimens was determined by immersing them in mercury prior to drying and weighing the fluid displaced.

The degrees of saturation (S_r) were computed from the dry density and water content determined in the laboratory, taking a value for the water density of 1 g/cm^3.

The pore size distribution was determined by mercury intrusion porosimetry (MIP). This technique allows the determination of the pore size distribution by injecting mercury into the sample at different pressures while controlling the volume intruded. The pressure applied may be related to the minimum pore diameter intruded, taking into account the characteristics of the fluid. The ratio of the volume of mercury intruded (pore volume) to the applied pressure (which conditions the minimum pore diameter accessed) allows distribution curves to be obtained establishing the percentage of pores of a size included within a given range.

Two pieces of each sample were used: a spare fragment resulting from the sample preparation and a fragment from the sample at the end of the gas permeability test. To remove the water of the samples prior to MIP testing they were lyophilised. The porosimeter used was a Micromeritics AutoPore Series IV 9500, which allowed the exploration of pore diameters between 0.006 and 600 μm.

4. Results

Nineteen gas permeability tests were performed in triaxial cells with bentonite samples obtained by on-site drilling of the bentonite barrier. The dry density of the samples was between 1.64 and 1.51 g/cm^3 and the water content between 29 and 19% (S_r between 79 and 104%). In each sampling section (Fig. 1) gas testing was carried out in samples taken at the same distance from the gallery wall drilled in the middle of a block (sound samples) and between two blocks (samples with interface). This way, at least six samples per section were tested, two from each barrier ring (external, middle and inner, Fig. 2), half of which had an interface along them. The comparison of the results obtained in both kinds of samples (with and without interface) should allow to assess the role of the interface on gas transport. Some of the results obtained in sound samples were presented in Carbonell et al. (2019), but are given here again for completeness. Out of the samples tested, eight had been drilled between two blocks and consequently had an interface along them. The characteristics of each sample tested, the pressure path followed and the detailed results obtained were reported in Villar et al. (2018a) and summarised in Tab. SM1. As an example, the results obtained in two of these samples are described in detail in the following sections. Afterwards, specific aspects of the results obtained in all the samples are discussed.

The samples were not artificially saturated prior to gas testing. Most samples were initially tested in the low-pressure setup and then in the high-pressure setup, where the pressure paths described in section 3.3.2 were approximately followed. The precise pressure paths depended on the characteristics of the samples and consequently were quite heterogeneous.

When flow occurred under a given pressure situation, the duration of the steps was generally short (1−2h). In many cases it was observed that, if the same pressure situation was kept for longer, flow decreased and the permeabilities computed were lower. This aspect has not been analysed in detail but could have some effect on the results obtained.

4.1. Sample BC-47-4

Sample BC-47-4 was drilled on site from section S47 (Fig. 1) between two blocks of the middle ring of the bentonite barrier (Fig. 2), hence the core had a longitudinal interface. Although the interface was not initially visible, upon trimming of the sample the two parts of it detached, likely as a result of the pressure relief (Fig. SM4). The initial dry density and water content of the specimen once trimmed were 1.59 g/cm^3 and 24.8%, respectively.

This was one of the first samples tested and was only tested in the high-pressure, unsteady-state (HP-US) equipment, following an unusual pressure path that consisted of these phases (represented also in Fig. SM5):

- Phase 1: the injection pressure was set to values between 0.1 and 0.3 MPa and the confining pressure was increased from 2 to 7 MPa; afterwards, keeping constant this confining pressure, the injection pressure was increased up to 2.5 MPa.
- Phase 2: the confining pressure was increased from 7 to 9 MPa.
- Phase 3: the confining pressure was decreased from 9 to 3 MPa and then the injection pressure was decreased to 1.5 MPa.

The permeability was computed from the evolution of pressure in the upstream and downstream pressure cylinders. The duration of most of the steps was between 1 and 3 days, although there were some steps that took very long, and thus the total duration of the test was of 172 days. The permeability values computed from the pressure increase in the downstream pressure cylinder are shown in Fig. 5 as a function of the injection pressure for different confining pressures. In this case the effect of injection pressure on permeability was not clear: for a constant confining pressure and for injection pressures lower than 0.8 MPa, permeability decreased as injection pressure increased, but above this value, the permeability remained constant or slightly increased. The duration of the steps could also have an influence on the permeability measured, since it decreased noticeably when the confining pressure was applied for a long time. Indeed the permeability decreased as the confining pressure increased, although with a dispersion that can be explained by the effect of injection pressure (which was not the same in all the steps), different duration of the steps and hysteresis on loading-unloading cycles. However, when the confining pressure decreased

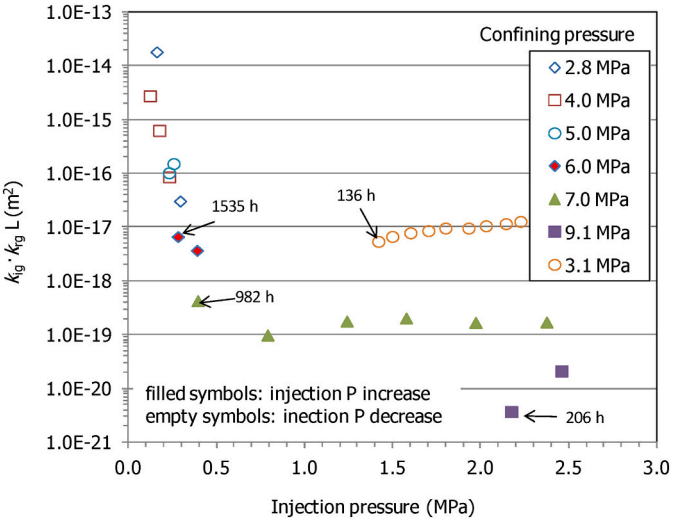

Fig. 5. Gas permeability at constant confining pressure for sample BC-47-4 (the duration of longer steps is indicated in hours.) Confining pressure was changed in the order indicated in the legend.

down to 3 MPa after loading up to 9 MPa, the permeability values measured were lower than the values measured initially for similar or even higher confining pressures. This would mean that some irreversible closure of gas pathways took place during consolidation. In fact, the interface between the two halves of the specimen appeared completely sealed at the end of the test (Fig. 6), and split only after drying in the oven.

4.2. Sample BC-53-2

This core sample from section S53 was drilled on site between two blocks in the inner ring of the barrier, hence it had a longitudinal interface along the core. Although the interface was not initially visible, after drying at the end of the test to determine the final water content of the sample, the two parts of the core split open (Figure 7:). The initial dry density of the sample was 1.63 g/cm^3 and the water content 22.5%, corresponding to a degree of saturation of 93%.

The sample was first tested in the low-pressure equipment (LP), under confining pressures of 0.6 and 1.0 MPa. The pressure decrease in the upwards cylinder and the permeability values computed from it are shown in Fig. 8. For a confining pressure of 0.6 MPa the gas permeability tended to increase towards the end of the test, which could indicate that certain drying took place because of the gas flow.

Afterwards, the sample was tested in the high-pressure steady-state equipment starting with the last confining pressure applied in the LP equipment, 1.0 MPa. The stress path followed in this test consisted of these phases (plotted in Fig. SM6):

- Phase 1: the test started at a confining pressure of 1.0 MPa and 0.2 MPa of injection pressure. The injection pressure was increased from 0.2 to 0.4 MPa, keeping constant confining pressure.
- Phase 2: the confining pressure was increased from 1.0 to 5.0 MPa, keeping an injection pressure of 0.4 MPa.
- Phase 3: unloading of the sample to a pressure as low as the initial value.

During the increase of injection pressure from 0.2 to 0.4 MPa in Phase 1, the gas permeability remained constant. However, the increase of confining pressure in Phase 2 caused a clear decrease of gas permeability. Fig. 9 shows the effect of confining pressure on gas permeability in both setups. The increase of confining pressure from 1 to 5 MPa caused a progressive decrease of flow until no measurable flow took place for a confining pressure of 5 MPa. Then, the sample was unloaded. During this phase, there was no measurable flow until the confining pressure decreased to 2 MPa, when the gas permeability computed was an order of magnitude lower than that for the same confining pressure during loading. This would indicate that the consolidation effect was irreversible. In fact, the dry density increased during the test from 1.63 to 1.64 g/cm^3.

4.3. Effect of injection and confining pressures

The effect of injection pressure on permeability in the range of pressures tested was for most samples negligible, as the two examples detailed above illustrated. In fact, the values measured under different injection pressures for a given confining pressure were similar among them and to the apparent gas permeability of each sample computed applying the Klinkenberg correction (Villar et al., 2018a). This would mean that the Klinkenberg effect was not relevant in the range of pressures applied, since they probably were high enough and there was no slippage contribution to gas flow. In contrast, in the case of some samples with the highest water content and lowest suctions, the increase in injection pressure caused a clear increase in gas permeability. It was checked that for these samples flow was not linearly related to the difference of squared pressures along the sample (P_{up} and P_{dw} in Eq. 8), which indicates that Darcy's law should not strictly be applied to compute permeability (Villar et al., 2018a; Carbonell et al., 2019). Examples of linear and non-linear relations between flow and P_{up}^2-P_{dw}^2 are shown in Fig. SM7.

Taking this into account, the average values of gas permeability measured for consecutive steps of different injection pressure under the same confining pressure have been plotted in Fig. 10 to Fig. 12, for samples of the three sampling sections shown in Fig. 1. After reaching the maximum confining pressure, corresponding to a value above which no measurable flow took place, the samples were progressively unloaded. Exceptionally, in sample BC-53-1 the maximum confining pressure (2.2 MPa) was determined by a technical failure and not by flow cessation.

The distance to the gallery axis is indicated in the legend of the figures. Distances about 100 cm indicate that the sample was taken from the external ring of the barrier (the radius of the gallery was 114 cm), values around 80 cm correspond to samples taken from the middle ring and values around 60 cm correspond to samples taken from the inner ring, the one closest to the heater.

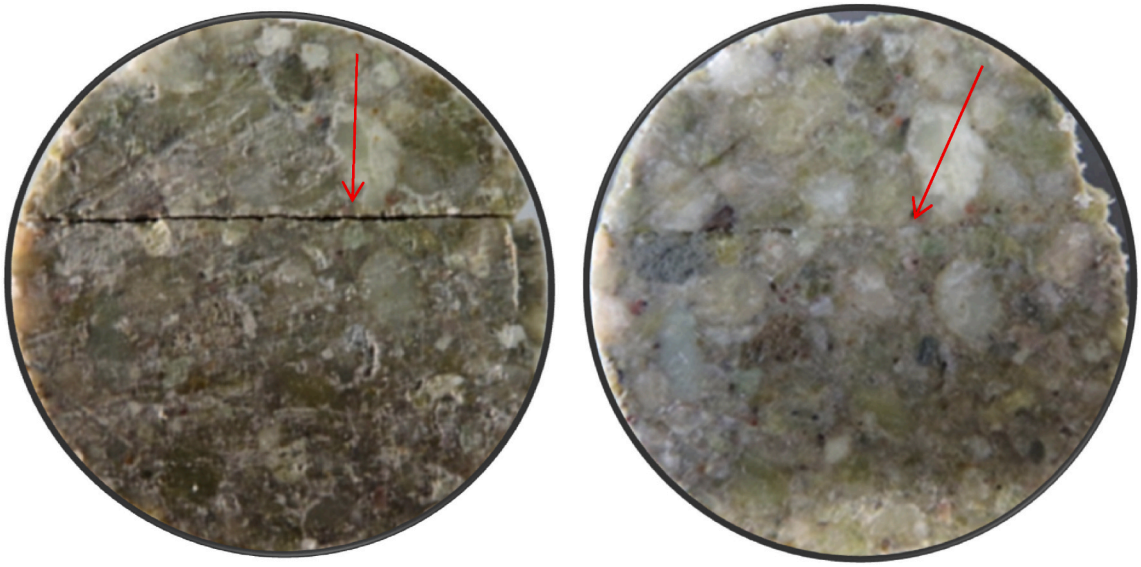

Fig. 6. Initial and final appearance of sample BC-47-4 (the arrows indicate the same position before and after testing).

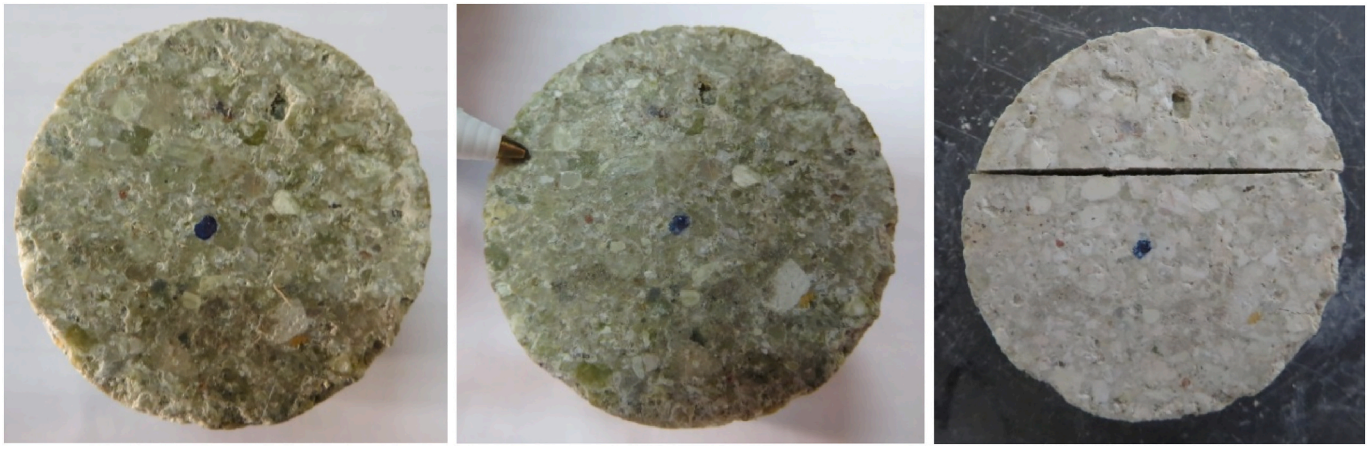

Fig. 7. Appearance of sample BC-53-2 before (left) and after (middle) gas testing. The interface split only after drying in the oven (right).

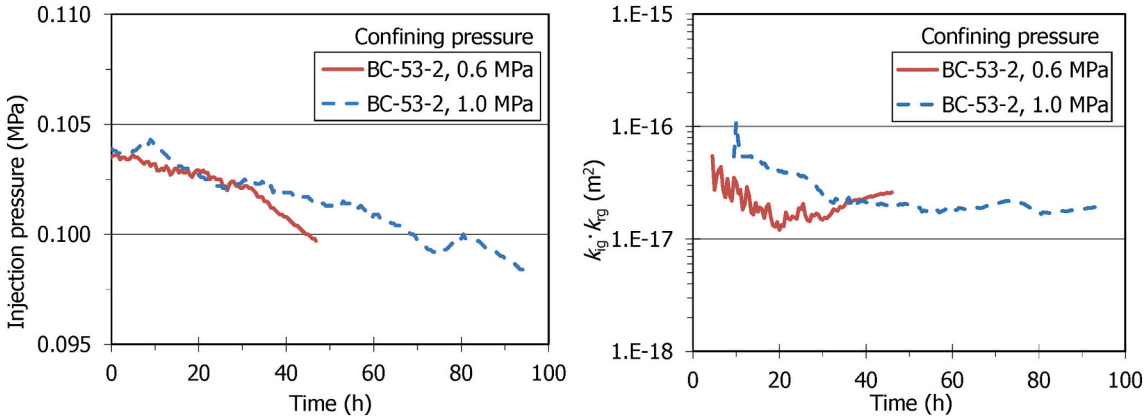

Fig. 8. Evolution of injection pressure and gas effective permeability ($k_{ig} \cdot k_{rg}$) in the low pressure equipment (LP) for sample BC-53-2 (injection gas pressure given in relative values).

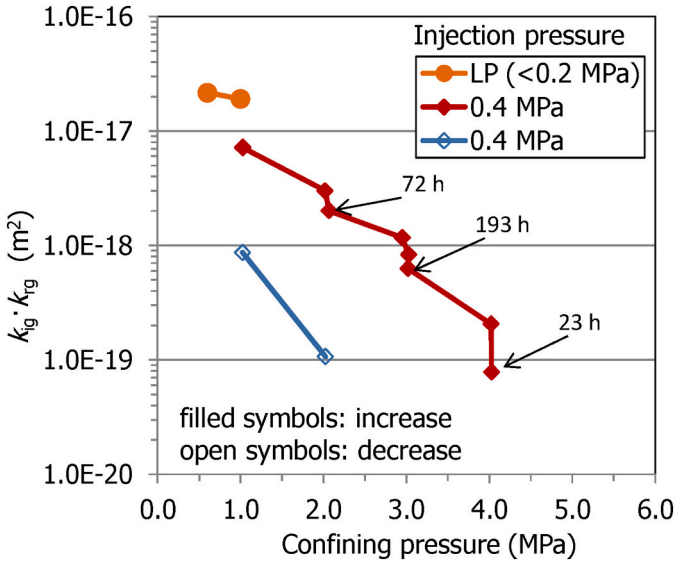

Fig. 9. Evolution of gas effective permeability at constant injection pressure (Phase 2 and 3) for sample BC-53-2. The duration of the longer steps is indicated.

For all the confining pressures applied the effective gas permeability decreased from the inner part of the barrier towards the granite in all sections. Indeed, the samples taken from the external ring of the barrier had the highest water contents and lowest dry densities. Overall, the samples closest to the heater, which were drier and had lower degrees of saturation (<90%), showed higher gas permeability. Section S53, which was close to the back end of the heater (Fig. 1), had overall higher water content than the sections in the middle part of the heater, where the temperatures were higher (Villar et al., 2020a). As a result, the samples from the inner ring of section S53 had higher degrees of saturation than in the other sections (S_r > 90%), and the permeability of these samples was in the order of the permeability of the samples taken from the middle and external rings of the other sections (Fig. 12).

The samples with interface tended to have higher permeability than sound samples taken at the same distance from the axis, particularly in the case of the inner ring. For example, the comparison between samples BC-47-3 (no interface, S_r = 97%) and BC-47-4 (interface, S_r = 95%) in Fig. 11 shows that the permeability of the sound sample was several orders of magnitude lower than that of its interface-sample counterpart, tested under a higher confining pressure. Although they were not tested under the same confining pressure, it is reasonable to assume that the permeability of sample BC-47-4 would be even higher for a lower confining pressure and consequently that under similar conditions the permeability of the sample with interface would be higher than that of the sample without interface. In the samples from the external and middle rings of the barrier the difference between samples with or without interface was not so evident, except for the sample BC-53-4,

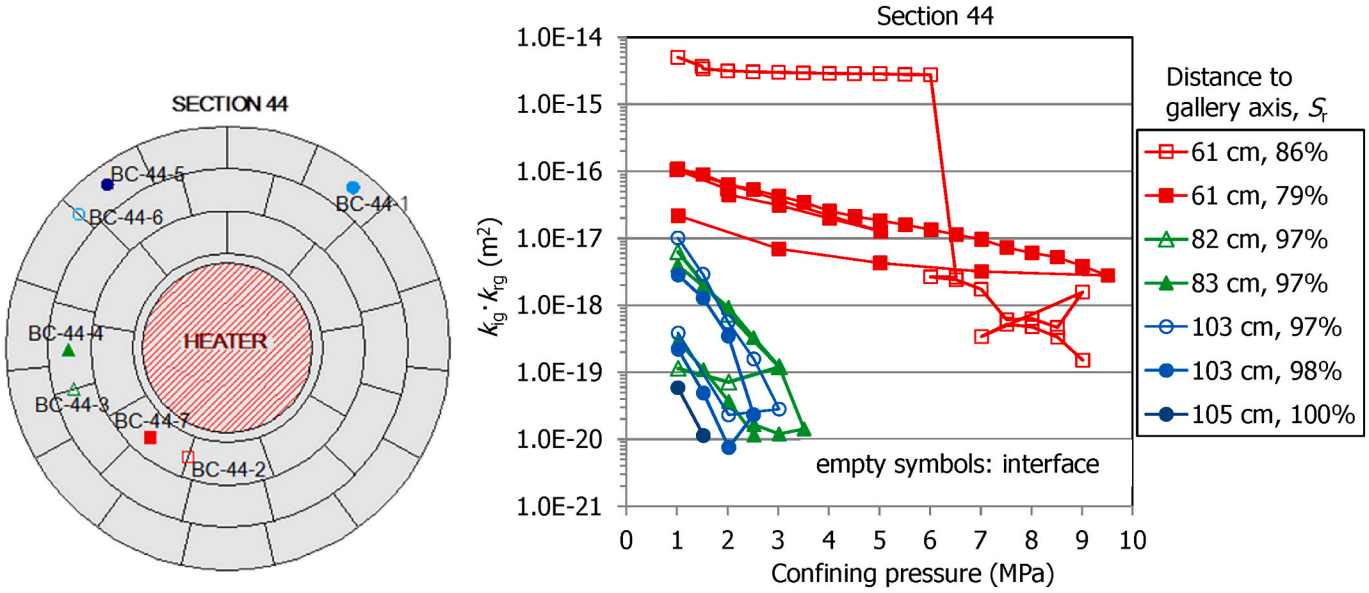

Fig. 10. Change of effective gas permeability with increase/decrease of confining pressure for samples from section S44 (flow was not steady in sample BC-44-5).

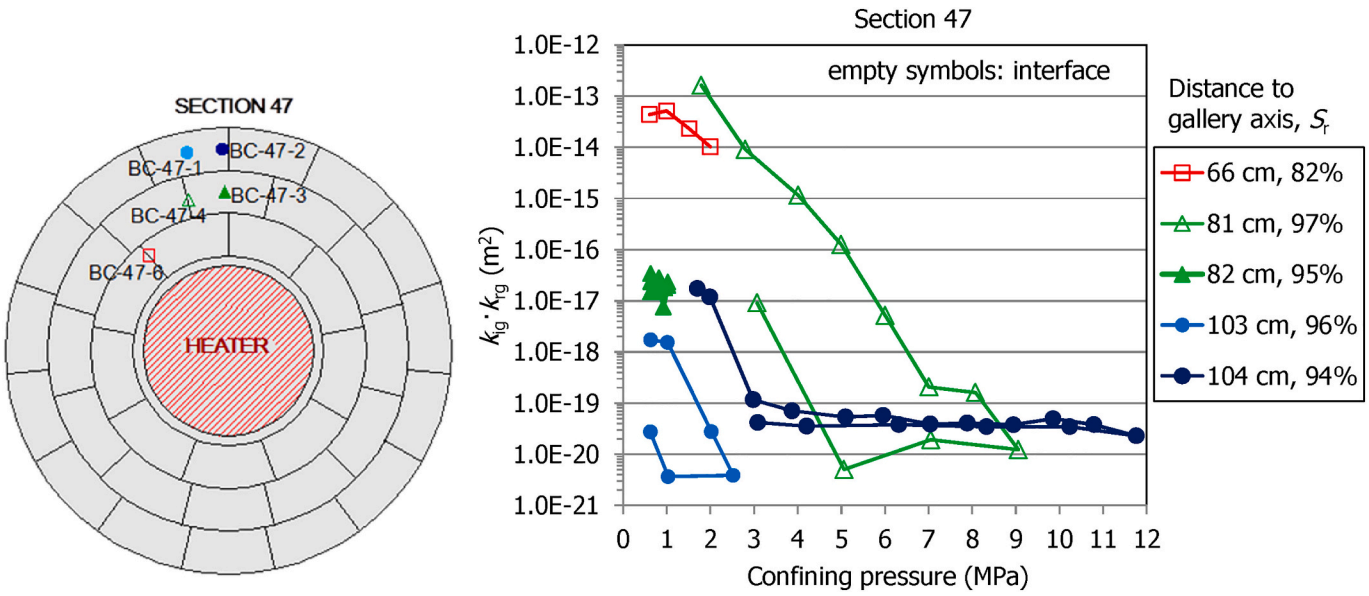

Fig. 11. Change of effective gas permeability with increase/decrease of confining pressure for samples from section S47.

which showed higher permeability than expected. This was a highly saturated sample taken from the external ring of section S53, whose interface was clearly visible during the preparation of the sample and quite open before testing (Fig. 3). As a result, there would be more mechanical interference between the two confronting sides, since the rugosity of the two halves would not exactly coincide after they were separated and then put together again for the test. Sample BC-47-4 (see section 4.1), which had an initially open interface, also recorded a very high permeability that drastically decreased with the increase in confining pressure (Fig. 11).

The decrease of gas permeability with confining pressure was significant. For confining pressures below 4 MPa most samples experienced a significant decrease in permeability as the confining pressure went on increasing. For higher confining pressures the decrease was less substantial, except when the sample had an interface. No flow took place through the samples from the external and middle rings, those more saturated, for confining pressures higher than 3–4 MPa. In contrast, for the sample of the internal ring from section S44 (BC-44-7), the confining pressure had to be increased up to 9.5 MPa to stop flow.

The permeability of samples with interface decreased steeply as the confining pressure increased. The permeability of sample BC-47-4, decreased four orders of magnitude when the confining pressure increased from 4 to 7 MPa, and sample BC-53-4, which had a similar degree of saturation in section S53, showed an analogous behaviour. The behaviour of sample BC-44-2, drilled between two blocks of the internal ring of section S44, was different, since its permeability barely changed as the confining pressure was increased to 6 MPa, but decreased three orders of magnitude when this value was exceeded, which probably indicates the closure of the interface.

Overall, the samples that had higher initial permeability –either because their degree of saturation was low or because they had an interface– had to be submitted to higher confining pressures to stop flow. During unloading, as the confining pressure decreased the effective permeability increased, but the original values were never recovered.

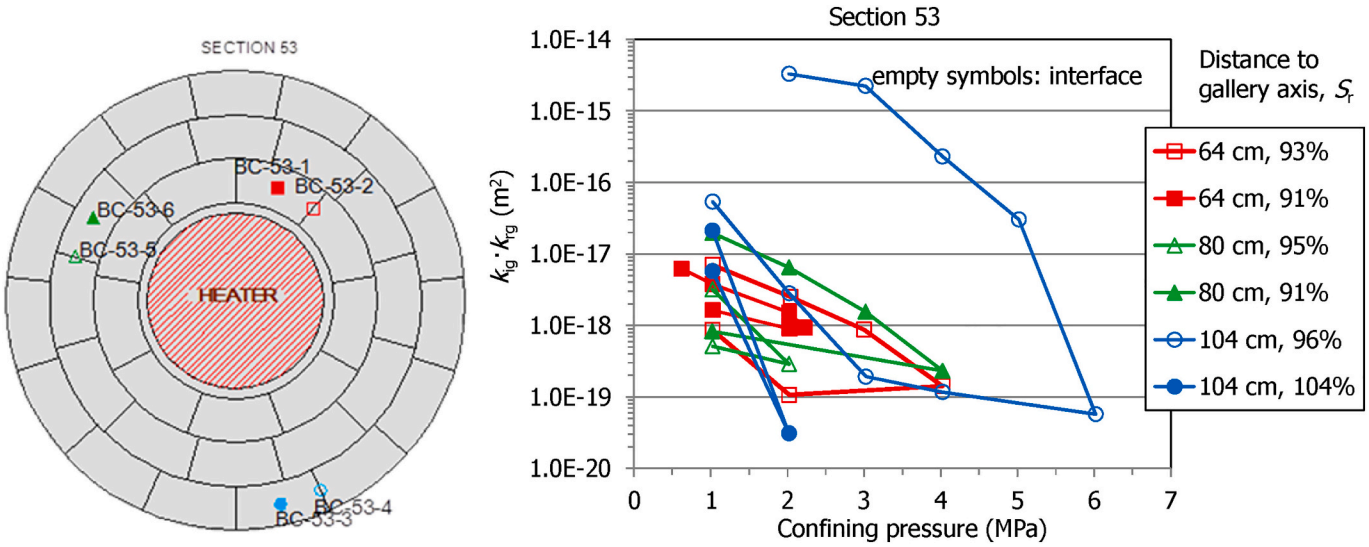

Fig. 12. Change of effective gas permeability with increase/decrease of confining pressure for samples from section S53 (flow was not steady in sample BC53-3).

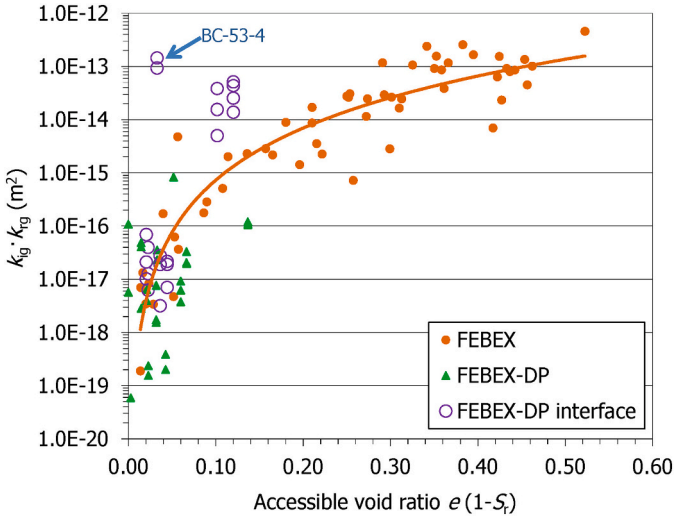

Fig. 13. Gas permeability as a function of the accessible porosity for the reference FEBEX bentonite (Eq. 3) and for FEBEX-DP samples with and without interface tested under confining pressures of 0.6 and 1.0 MPa (modified from Carbonell et al., 2019).

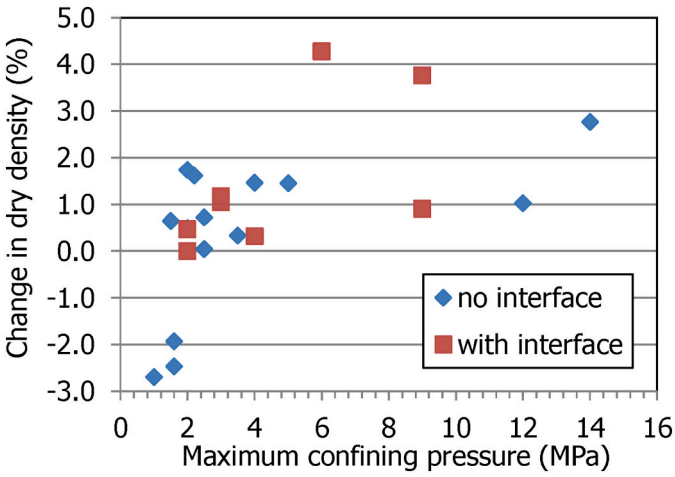

Fig. 14. Change in dry density occurred during gas testing as a function of the maximum confining pressure applied during the tests (positive values indicate increase).

The irreversibility of this change was more noticeable in the samples with interface.

4.4. Comparison with the reference bentonite

The gas permeability of the reference FEBEX bentonite samples, compacted to different dry densities with various water contents, was measured in previous researches and the correlation between accessible void ratio and gas effective permeability shown in Eq. 3 was obtained for samples with degrees of saturation lower than 97%. Those results and the ones obtained in the FEBEX-DP samples summarised in the previous section have been plotted in Fig. 13. These values were obtained in the same setups as the values obtained for the reference sample. In order to make the results strictly comparable, only those values obtained under confining pressures of 0.6 and 1.0 MPa have been represented. Nevertheless, it was observed that, for any of the confining pressures applied, the permeability tended to be higher the higher the accessible void ratio (Villar et al., 2018a). The accessible void ratio of the FEBEX-DP samples were overall very low (below 0.15), in the low range of the FEBEX samples, because their degree of saturation was very high. Nevertheless, the new values obtained in samples submitted for 18 years to barrier conditions are consistent with those of the reference bentonite, or maybe in the lower range. The scatter in the data was high because the range of dry densities and water contents involved was large and there were also samples with and without interface.

For the higher values of accessible void ratio, the samples with interface had higher permeabilities than those computed with Eq. 3, whereas for the lower accessible void ratios there was not a clear difference between samples with or without interface, and both were closer to those of the reference bentonite. This was observed for all the range of confining pressures tested. An exception was sample BC-53-4, which was drilled in the external ring of the barrier and consequently had a low accessible void ratio, but showed higher permeability than expected, probably because of the exceptionally open interface at the beginning of the test, as discussed above.

4.5. Final state: microstructural changes

Final checking of water content along the samples showed that the

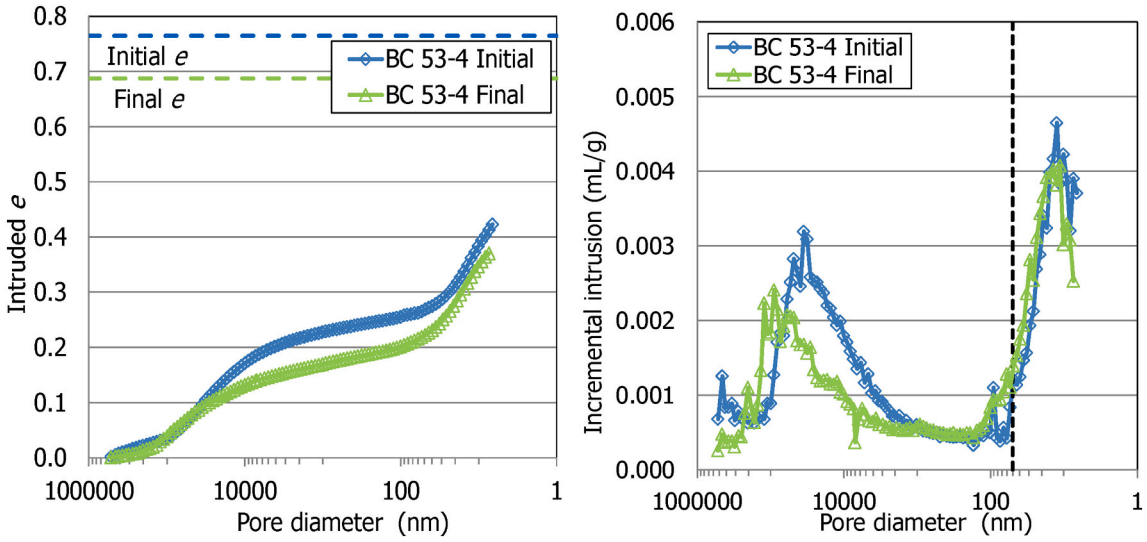

Fig. 15. Pore size distribution of sample BC-53-4 (S_r = 96%, distance to gallery axis 104 cm, with interface) before and after gas testing (the dotted vertical line indicates de separation between macro and mesopores).

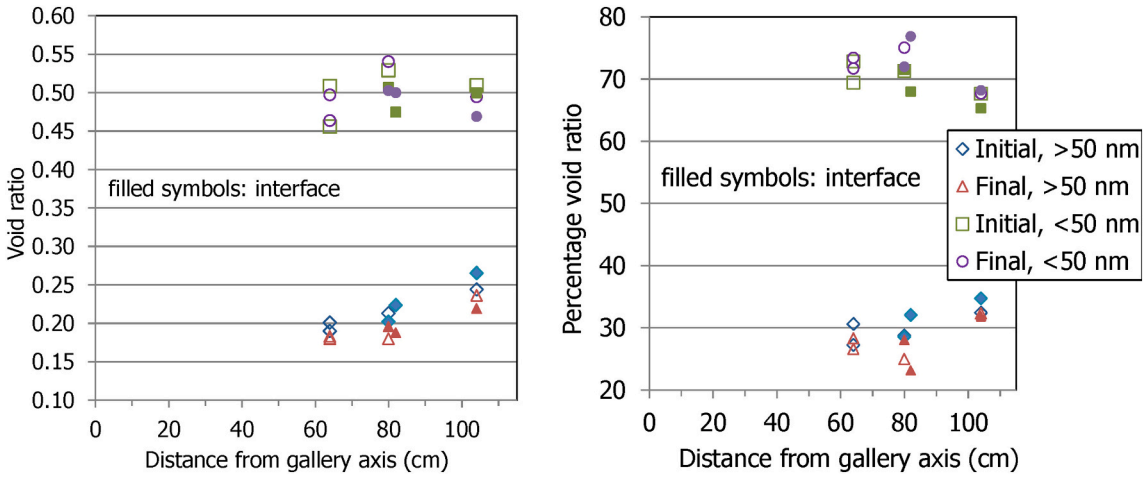

Fig. 16. Void ratio corresponding to pores larger and smaller than 50 nm of the bentonite samples before and after gas testing.

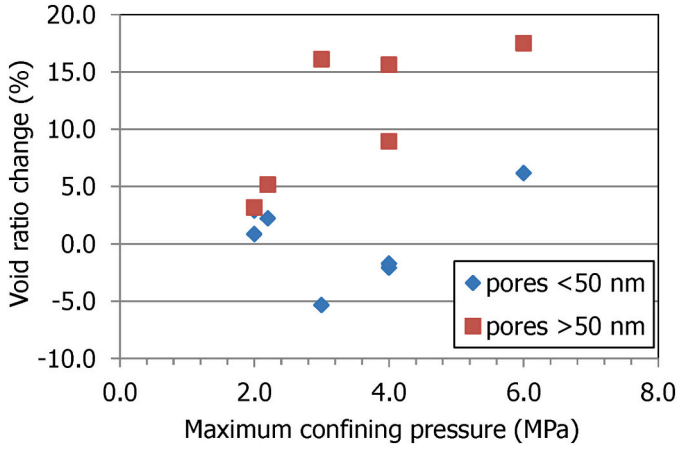

Fig. 17. Change in the void ratio corresponding to pores larger and smaller than 50 nm obtained by MIP after gas testing (positive values indicate decrease).

gravimetric water content was usually lower in the upper part, from where gas was injected (although the differences inside a given sample were lower than 0.5%). This indicates that certain drying of the upper part of the samples took place as a consequence of gas injection, the water being pushed by the gas towards the bottom of the samples. In some cases, particularly in the samples with higher initial water content, water could have been expelled out of the sample, because the final water content was found to be lower than the initial one (on average 3.2 ± 3.8%), both in samples with and without interface. However, no liquid water outflow was actually observed in any test. In fact, it cannot be ruled out that at least part of the decrease in water content at the end of the test observed in some samples could have taken place during the initial trimming process of the cores (see section 3.2).

At the end of the tests the dimension of the samples were measured and it was checked that, in most cases, the dry density of the samples had increased, which is consistent with the decrease in effective gas permeability occurred during the tests (section 4.3). The dry density of the samples increased after testing in all those tests in which the maximum confining pressure applied was higher than 2.5 MPa (except samples BC-47-1, BC-44-4 and BC-53-3). In fact, there is a positive linear correlation between the change in dry density and the maximum pressure applied (R^2 = 0.6), but the increase was more notable for maximum

confining pressures below 5 MPa (Fig. 14).

The pore size distribution of some of the samples was determined by mercury intrusion porosimetry before and after gas testing. A spare fragment resulting from the sample preparation and a fragment from the sample at the end of the test were used. The aim of these tests was to analyse the effect of gas flow on the pore size distribution of the bentonite.

The mercury intrusion method allows access to be gained only to part of the macroporosity (pores between 600 μm and 50 nm) and to part of the *meso*pores (those of sizes between 50 and 6 nm), since mercury does not intrude the microporosity (pores of a size of less than 2 nm, according to the classification of Sing et al., 1985). In the high-density clay materials retrieved from the FEBEX-DP, pores larger than those that can be quantified by MIP are not expected. Considering that most of the non-intruded porosity corresponds to the pores of a size smaller than the limit of the apparatus, an estimation of the percentage of pores actually intruded can be made by comparing the actual void ratio of the samples (e, computed from their dry density and density of solid particles) and the apparent void ratio calculated from mercury intrusion (e_{nw}, mercury being a non-wetting [nw] fluid).

The curves corresponding to a sample before and after gas testing are shown Fig. 15. The figure on the left shows the cumulative intruded void ratio. These void ratios have been corrected to take into account the percentage of pores not intruded by mercury. The total void ratio of the samples is indicated in the figure by dotted horizontal lines. The void ratio actually intruded was in all samples of only about 50%, which would mean that the percentage of pores smaller than 6 nm or not interconnected was very relevant. All the samples experienced certain decrease in void ratio (increase in dry density) after gas testing, which is attributed to the compression exerted by the confining pressure applied (Fig. 14). The figure on the right shows the incremental mercury intrusion over the range of pore sizes explored in the tests. Two pore families appeared systematically in all the samples, one in the size range of macropores and another one in the size range of mesopores. Overall the curves before and after gas testing were similar for each sample, and only the samples from the external ring, with very high degrees of saturation (e.g. BC53–4 in Fig. 15), showed a clear increase in the size mode of the macropores after gas testing (Villar et al., 2018a).

From these curves, the void ratio corresponding to pores of diameter higher or smaller than 50 nm (i.e. macropores and meso+micropores), can be obtained. The results have been plotted in Fig. 16 as a function of the distance to the gallery axis of the sample. There was an overall decrease in the macropore void ratio after gas testing, whereas the void ratio corresponding to pores <50 nm did not clearly change. In terms of the proportion of total void ratio corresponding to each of these pore sizes, the percentage of macropores decreased after gas testing while the percentage of pores <50 nm increased. Hence, the increase in dry density observed in most samples after gas testing (Fig. 14) would have been achieved by the decrease in macropore volume. The interfaces did not seem to affect these pore size distribution changes. Concerning the size of the pores, in the samples from the external ring the size of the macropores increased after gas testing, which could be connected with the opening of pathways, because the accessible void ratio in these samples was very low. In contrast, the size of the mesopores did not change in a clear consistent way during gas testing.

The percentage of void ratio change occurred during gas testing for pores larger and smaller than 50 nm is shown in Fig. 17 as a function of the maximum confining pressure reached during gas testing. The higher the confining pressure applied the higher the decrease in macropore void ratio, whereas smaller pores did not seem to change coherently with confining pressure. These results agree well with the change of dry density as a consequence of the confining pressure applied during gas testing, which was significant for confining pressures higher than 2 MPa. Since the samples for which the pore size distribution was analysed had been subjected to confining pressures higher than this value, the total void ratio, and particularly the void ratio corresponding to macropores, decreased in all of them.

5. Discussion

In the previous sections results of the gas permeability measurements performed in samples retrieved from the FEBEX in situ tests have been presented. The water content and dry density of the bentonite changed across the barrier as a function of the distances to the heater and the granite. Consequently, the samples taken closest to the heater had lower water content and higher dry density, whereas the samples taken closest to the granite had the highest water content and lowest dry density. The effective gas permeability of the samples decreased with the increase of water content and the decrease in dry density and tended to be lower towards the granite, where the degree of saturation was higher.

During the tests, the gas flow observed was steady in most cases and no effect of the injection pressure on the permeability values was detected, except for a few of the more saturated samples, for which gas permeability increased with increasing gas injection pressure (in fact this behaviour was clear only in sample BC-53-3), indicating non-Darcian flow. Additionally, it was checked that the Klinkenberg effect was not significant in the range of pressures applied (Villar et al., 2018a).

However, the gas permeability was clearly affected by the stress state. It decreased noticeably with the increase in confining pressure up to 4 MPa, particularly for the wetter samples, those taken closer to the granite. Beyond a confining stress of 9 MPa no gas flow took place through any of the wetter samples, hence the breakthrough pressure for them would be higher than this value, which in turn is higher than the expected swelling pressure (Eq. 2). In fact, gas breakthrough pressures higher than the swelling pressure were measured in the FEBEX reference bentonite compacted and tested under isochoric conditions (Gutiérrez-Rodrigo et al., 2021). In contrast, flow took place through the drier samples, even for confining pressures as high as 9 MPa. The consolidation induced by the increase in confining pressure increased the degree of saturation of the samples and reduced their suction, taking them back to a stress state closer to that in the barrier during the in situ test. At the end of operation of the FEBEX in situ test total pressures above 2 MPa were measured in the intermediate bentonite ring and higher than 5 MPa in the outer part of the barrier (Martínez et al., 2016; Villar et al., 2020b), and this could indicate that during operation the stress state in the barrier was high enough as to limit gas migration.

The confining stress reduced the size of the gas pathways, also increasing their tortuosity. In the case of the less saturated samples there was insufficient moisture to reduce or block the air-filled pore network of the specimens and minimise gas flow, and the gas found ways out until the confining pressure was enough to sufficiently reduce the air-filled pore space. In contrast, in the highly-saturated samples there was no need of applying a high confining pressure to completely block the air passages, which already were small and tortuous. This also would explain the fact that the effect of injection pressure increase was only noticeable in the samples with the highest water content, in which small changes in the size of the cross-section of the gas pathways would trigger significant changes in very low permeability.

The decrease in permeability occurred during loading was not reversible, and the gas permeability of the samples after unloading was lower than the initial one. Most of the samples experienced during operation in the barrier an increase in void ratio as a result of hydration and swelling, which led to the reduction of the initial dry density of the blocks (1.7 g/cm^3) to the average dry density of the barrier (1.6 g/cm^3). Consequently the apparent preconsolidation stress of the bentonite decreased during in situ operation, whereas the pre-yield and post-yield compressibility values increased (Romero et al., 2017, included in Villar, 2017). This would explain the fact that the samples consolidated easily during gas testing. In fact, the dry density of the samples at the end of the tests in which confining pressures higher than 2 MPa were applied was higher than the initial one.

The pore size distribution analyses carried out by mercury intrusion porosimetry showed a decrease in the macropore void ratio in all the samples tested applying confining pressures higher than 2 MPa. This decrease was more significant as the confining pressure applied during gas testing was higher, which would mean that the compression exerted by the confining pressure was mostly absorbed by the macropores. In some of the wetter samples an increase of the size of the macropores was observed after gas testing, which could correspond to the opening of pathways allowing gas flow, given the very low accessible void ratio of these nearly saturated samples. Gonzalez-Blanco et al. (2016a, 2016b) observed a new family of pores at entrance sizes larger than 2 μm after gas injection in samples of argillaceous rock formations. These pores were associated with fissure opening and would act as preferential air pathways. They were observed by microcomputed tomography, both in a clay rock (Gonzalez-Blanco et al. 2017a) and in bentonite (Gonzalez-Blanco et al., 2017b). Harrington et al. (2017) analysed the stress field measured during a gas injection test in saturated compacted bentonite and inferred from it that the gas pathways were created by dilatancy and propagated through the clay in response to variations in applied gas pressure.

The gas permeability of the FEBEX reference bentonite is mainly related to the void ratio accessible for gas flow, $e(1\text{-}S_r)$, which depends on water content and dry density (see section Background: gas transport studies in FEBEX bentonite). For the FEBEX-DP samples, because of the high water saturation of most of the barrier after the long operation period, the accessible void ratio was below 0.15, and decreased towards the external part of the barrier, where the degree of saturation was higher. For these samples the decrease of gas permeability with accessible void ratio roughly followed the empirical relation of Eq. 3, which predicts an acute decrease of gas permeability in the low range of accessible void ratios. In fact, the drop in effective gas permeability when approaching full saturation is that of several orders of magnitude (Fig. 13). Therefore, it seems that no changes on the gas transport properties of the bentonite matrix took place during operation.

However, samples with an interface drilled in the internal ring of the barrier had higher permeability than samples of similar accessible void ratio with no interface, and it was necessary to apply higher confining pressures to reduce or suppress gas flow in them. In fact the presence of an interface had higher relevance than the accessible void ratio on the gas permeability, probably because the gas transport mechanisms in both kinds of samples were not the same: flow took place through the accessible porous structure, but in the samples with interface it preferentially occurred along the interface, likely following "models" of flow in deformable rock fractures, in which liquid flow takes place according to a local cubic law or its variations. The sudden decreases in permeability occurred in some samples when confining pressure was increased beyond a given value would correspond to the closing of the interface as a preferential pathway. In contrast, wetter samples drilled along interfaces of the intermediate and external rings of the barrier (which had very low accessible void ratio, lower than 0.08, because of the high saturation), had permeabilities closer to those corresponding to the same accessible void ratio in the reference bentonite. In fact, in these samples the interfaces were barely visible and looked like sealed before gas testing.

Popp et al. (2014) tested the interface between blocks manufactured from a bentonite/sand (60/40) mixture. Under dry conditions, gas flow along the interfaces was at least four orders of magnitude higher than through the matrix. An increase in confinement significantly lowered the gas flow but the effect was more pronounced for interfaces than for the matrix. They saturated the blocks assemblages and performed gas injection and shear tests to check the behaviour of the interface. The authors concluded that the interface perfectly healed after saturation, which was physically verified by the development of cohesion after saturation. All these observations are consistent with the findings reported in this work. Gas breakthrough tests performed in saturated samples of FEBEX bentonite under isochoric conditions showed that samples with an interface behaved as samples of the same dry density with no interface, finding in both cases breakthrough pressure values related to dry density. The conclusion was that after material homogenization the interface was not a preferential pathway, neither for water nor for gas (Gutiérrez-Rodrigo, 2018; Gutiérrez-Rodrigo et al., 2021).

Previous laboratory studies showed that, in the FEBEX compacted bentonite, two-phase flow through stable pathways seemed to take place for degrees of saturation lower than about 97%, since in these samples gas flow was stable for a given pressure gradient. For higher degrees of saturation pathway dilation could be the predominant mechanism (Villar et al., 2013; Gutiérrez-Rodrigo, 2018). Graham et al. (2002) found that this threshold was 93% for a sodium bentonite, and that below this degree of saturation there was only small resistance to gas migration. Tests performed in compacted saturated samples under isochoric conditions showed that the threshold pressure for gas entry into the bentonite was higher than the swelling pressure and seemed to be lower than the gas pressure required for fracturing (macroscopically) the material (Gutiérrez-Rodrigo et al., 2021). In contrast, in the research reported here, two-phase flow seems to have taken place in most cases, even for samples with degree of saturation higher than 97%. The fact that these samples were tested under constant confining stress (in triaxial cells) instead of under no volume change conditions (isochoric), would have made easier the transport of gas, with opening of trajectories for gas flow that could not be opened under isochoric conditions. Hence, the testing conditions seem to have an influence on the results obtained. Graham et al. (2016) concluded from gas injection tests in saturated compacted bentonite that the degree of compressibility of the clay and the stress conditions may be an important control on the approach to gas breakthrough in the buffer. In this line, Xu et al. (2015) performed laboratory tests in a saturated, low permeability clay that showed that the failure of the sealing efficiency was closely related to the difference between the gas injection pressure and the confining pressure.

6. Concluding remarks

The FEBEX in situ test reproduced the engineered barrier system of an underground repository for nuclear waste and was running under natural hydration from the granitic host rock and heating from the simulated canister, for 18 years. The barrier was composed of bentonite blocks and had an average dry density of 1.6 g/cm^3. In 2015 the heater was switched off, the experiment was dismantled and bentonite samples were taken at different positions around the heater. Some of these samples were drilled between two blocks, therefore they had an interface along the core. The gas permeability of the samples was measured in custom-built setups using nitrogen as gas, without artificially saturating the samples prior to or during gas testing, and checking the effect of injection and confining pressures.

Except for some of the most saturated samples, stable gas flow took place for any of the boundary conditions applied. The reduction of gas permeability with confining pressure resulted from the decrease in the volume of macropores, and was particularly significant for the more saturated samples, i.e. those from the external part of the barrier. Higher gas permeability values were measured in the samples taken close to the heater, which were drier, and particularly in those with interface. However, the gas permeability of the more saturated samples was related to the gas accessible void ratio (related in turn to bentonite water content and dry density), irrespective of the presence of interface, which attest the healing of the contacts between blocks as a result of saturation.

The effective permeability values obtained are probably conservative, since they were obtained for stress situations maintained for relatively short periods of time (a few hours), whereas in some cases it was checked that gas permeability was lower if the samples were compressed for longer periods of time. It is also possible that temperatures in the range of those expected around the canisters of a real repository have an effect on gas permeability, and this aspect has not been checked, since all the measurements were performed at laboratory temperature.

The results obtained suggest that the gas generated in the proximity to the waste containers would be able to move by advection as long as the bentonite around it remains unsaturated, more easily along interfaces. However, it is likely that in a real repository even the drier interfaces in the internal part of the bentonite barrier would not be preferential gas pathways once the external part of the barrier is saturated, because the high stresses in the system would close them. In any case, the external, fully saturated part of the barrier would block gas movement away from the barrier, and gas would only be able to escape slowly by diffusion in the pore water or suddenly by breakthrough if gas pressure builds up above a value that would be higher than the swelling pressure but very dependent on the stress conditions. The role of the interfaces on gas transport would only be relevant for low degrees of saturation, i.e. at the beginning of operation or close to the heater. Nevertheless, since gas generation would be triggered by processes implying high water contents, it is not expected to be relevant until advance stages of the repository life, when the interfaces between blocks in all the barrier will have been sealed as a result of full saturation.

Declaration of Competing Interest

The authors declare that they have no known competing financial interests or personal relationships that could have appeared to influence the work reported in this paper.

Acknowledgements

The research leading to these results was financed through the Annex XLII of the ENRESA-CIEMAT framework agreement and by the FEBEX-DP consortium (NAGRA, SKB, POSIVA, CIEMAT, KAERI.) The preparation of this paper was performed in the framework of the EURAD project – WP6 GAS (http://www.ejp-eurad.eu/), which receives funding from the European Union's Horizon 2020 research and innovation programme under grant agreement No 847593. Part of the laboratory work was carried out by J. Aroz, R.J. Iglesias, and F.J. Romero. The control and data acquisition systems for the gas permeability tests were developed by Dr. J.M. Barcala of CIEMAT. The mercury intrusion porosimetry tests were performed at the Petrophysical laboratory of CIEMAT by N. Brea, supervised by Dr. R. Campos. Beatriz Carbonell was hired in the framework of the Spanish National System of Youth Guarantee in R+D 2014, with financing of the European Social Fund and the Youth Employment Initiative.

Appendix A. Supplementary data

Supplementary data to this article can be found online at https://doi.org/10.1016/j.enggeo.2021.106087.

References

Bárcena, I., García-Siñeriz, J.L., 2015. FEBEX-DP (GTS) Full Dismantling Sampling Plan (in situ Experiment). Nagra Arbeitsbericht NAB 15-14, p. 103.

Carbonell, B., Villar, M.V., Martín, P.L., Gutiérrez-Álvarez, C., 2019. Gas transport in compacted bentonite after 18 years under barrier conditions. Geomech. Energy Environ. 17, 66–74. https://doi.org/10.1016/j.gete.2018.03.001.

ENRESA, 2006. FEBEX Full-scale Engineered Barriers Experiment, Updated Final Report 1994-2004. Publicación Técnica ENRESA 05-0/2006, Madrid, p. 590.

García-Siñeriz, J.L., Abós, H., Martínez, V., de la Rosa, C., Mäder, U., Kober, F., 2016. FEBEX-DP: Dismantling of the heater 2 at the FEBEX "in situ" test. In: Description of operations. Nagra Arbeitsbereicht NAB16-011, Wettingen, Switzerland, p. 92.

Gonzalez-Blanco, L., Romero, E., Jommi, C., Li, X., Sillen, X., 2016a. Gas migration in a Cenozoic clay: Experimental results and numerical modelling. Geomech. Energy Environ. 6, 81–100.

Gonzalez-Blanco, L., Romero, E., Li, X., Sillen, X., Jommi, C., 2016b. Air injection tests in two argillaceous rock formations: Experimental results and modelling. In: Proceedings of the 1st International Conference on Energy Geotechnics, ICEGT 2016, Kiel, Germany, 29–31 August 2016. CRC Press, ISBN 9781138032996, pp. 715–721. https://doi.org/10.1201/b21938-112.

Gonzalez-Blanco, L., Romero, E., Jommi, C., Sillen, X., Li, X., 2017a. Exploring Fissure opening and their connectivity in a Cenozoic clay during gas injection. In: Ferrari, A., Laloui, L. (Eds.), Advances in Laboratory Testing and Modelling of Soils and Shales (ATMSS), Springer Series in Geomechanics and Geoengineering. Springer, Cham, Switzerland, ISBN 978-3-319-52772-7, pp. 288–295. https://doi.org/10.1007/978-3-319-52773-4_33.

Gonzalez-Blanco, L., Romero, E., Marschall, P., 2017b. Pathway development and connectivity during gas injection/dissipation tests: experimental results and numerical modelling. In: Interpore 2017: 9th International Conference on Porous Media & Annual Meeting.

Graham, J., Halayko, K.G., Hume, H., Kirkham, T., Gray, M., Oscarson, D., 2002. A capillarity-advective model for gas break-through in clays. Eng. Geol. 64, 273–286.

Graham, C.C., Harrington, J.F., Sellin, P., 2016. Gas migration in pre-compacted bentonite under elevated pore-water pressure conditions. Appl. Clay Sci. 132-133, 353–365. https://doi.org/10.1016/j.clay.2016.06.029.

Gutiérrez-Rodrigo, V., 2018. Transporte de gas en materiales de barrera. Tesis Doctoral. Universidad Complutense de Madrid, p. 303. Colección Documentos CIEMAT. ISBN: 978-84-7834-802-2. Madrid.

Gutiérrez-Rodrigo, V., Villar, M.V., Martín, P.L., Romero, F.J., Barcala, J.M., 2015. Gas-breakthrough pressure of FEBEX bentonite. In: Shaw, R.P. (Ed.), Gas Generation and Migration in Deep Geological Radioactive Waste Repositories. Geological Society, London, Special Publications, 415, 47-57. https://doi.org/10.1144/SP415.4. First published online November 14, 2014.

Gutiérrez-Rodrigo, V., Martín, P.L., Villar, M.V., 2021. Effect of interfaces on gas breaktrough pressure in compacted bentonite used as engineered barrier for radioactive waste disposal. Process. Saf. Environ. Prot. 149, 244–257. https://doi.org/10.1016/j.psep.2020.10.053.

Harrington, J.F., Horseman, S.T., 2003. Gas migration in KBS-3 buffer bentonite: Sensitivity of test parameters to experimental boundary conditions. In: Report TR-03-02. Svensk Kärbränslehantering AB (SKB), Stockholm, Sweden.

Harrington, J.F., Graham, C.C., Cuss, R.J., Norris, S., 2017. Gas network development in a precompacted bentonite experiment: evidence of generation and evolution. Appl. Clay Sci. 147, 80–89.

Horseman, S.T., Harrington, J.F., Sellin, P., 1999. Gas migration in clay barriers. Eng. Geol. 54, 139–149.

Lloret, A., 1982. Comportamiento deformacional del suelo no saturado bajo condiciones drenadas y no drenadas. Ph. D. Thesis. Universidad Politécnica de Cataluña.

Loosveldt, H., Lafhaj, Z., Skoczylas, F., 2002. Experimental study of gas and liquid permeability of a mortar. Cem. Concr. Res. 32, 1357–1363.

Martínez, V., Abós, H., García-Siñeriz, J.L., 2016. FEBEX-e: Final Sensor Data Report (FEBEX In Situ Experiment). Nagra Arbeitsbericht NAB 16-019, Madrid, p. 244.

Olivella, S., Alonso, E.E., 2008. Gas flow through clay barriers. Géotechnique 58 (3), 157–176.

Ortiz, L., Volckaert, G., Mallants, D., 2002. Gas generation and migration in Boom Clay, a potential host rock formation for nuclear waste storage. Eng. Geol. 64, 287–296.

Popp, T., Rölke, C.Y., Salzer, K., 2014. Hydromechanical properties of bentonite-sand block assemblies with interfaces in engineered barrier systems. In: Shaw, R.P. (Ed.), Gas Generation and Migration in Deep Geological Radioactive Waste Repositories. Geological Society, London, Special Publications, 415, pp. 19–33.

Romero, E., Alvarado, C., Lloret, A., Mirsalehi, S., 2017. Laboratory tests on the post mortem hydro-mechanical characterisation of FEBEX bentonite. In: CIMNE-UPC-GEOLAB, p. 84.

Scheidegger, A.E., 1974. The Physics of Flow through Porous Media, 3rd ed. University of Toronto Press, Toronto.

Sellin, P., Leupin, O., 2013. The use of clays as an engineered barrier in radioactive-waste management – a review. Clay Clay Miner. 61 (6), 477–498. https://doi.org/10.1346/CCMN.2013.0610601.

Sing, K.S.W., Everett, D.H., Haul, R.A.W., Moscou, L., Pierotti, R.A., Rouquérol, J., Siemieniewska, T., 1985. Reporting physisorption data for gas/solid systems with special reference to the determination of surface area and porosity. Pure Appl. Chem. 57 (4), 603–619. IUPAC.

Villar, M.V., 2002. Thermo-hydro-mechanical characterisation of a bentonite from Cabo de Gata. In: A Study Applied to the Use of Bentonite as Sealing Material in High Level Radioactive Waste Repositories. Publicación Técnica ENRESA 01/2002, Madrid, p. 258.

Villar, M.V., 2017. FEBEX-DP Postmortem THM/THC Analysis Report. NAB 16-017, p. 143.

Villar, M.V., Lloret, A., 2001. Variation of the intrinsic permeability of expansive clay upon saturation. In: Adachi, K., Fukue, M. (Eds.), Clay Science for Engineering. Balkema, Rotterdam, pp. 259–266.

Villar, M.V., García-Siñeriz, J.L., Bárcena, I., Lloret, A., 2005. State of the bentonite barrier after five years operation of an in situ test simulating a high level radioactive waste repository. Eng. Geol. 80 (3–4), 175–198. https://doi.org/10.1016/j.enggeo.2005.05.001.

Villar, M.V., Gutiérrez-Rodrigo, V., Martín, P.L., Romero, F.J., Barcala, J.M., 2013. Gas transport in bentonite. In: Informes Técnicos CIEMAT 1301. Madrid, p. 63. https://doi.org/10.13140/RG.2.2.14334.28489.

Villar, M.V., Iglesias, R.J., Abós, H., Martínez, V., de la Rosa, C., Manchón, M.A., 2016. FEBEX-DP Onsite Analyses Report. NAB 16-012, p. 106.

Villar, M.V., Carbonell, B., Martín, P.L., Gutiérrez-Álvarez, C., Barcala, J.M., 2018a. Gas Permeability of Bentonite Samples of the FEBEX Dismantling Project (FEBEX-DP). Informes Técnicos CIEMAT 1431, Madrid, p. 89.

Villar, M.V., Iglesias, R.J., García-Siñeriz, J.L., 2020a. State of the in situ Febex test (GTS, Switzerland) after 18 years: a heterogeneous bentonite barrier after 18 years operation. Environ. Geotechn. 7 (2), 147–159. https://doi.org/10.1680/jenge.17.00093.

Villar, M.V., Iglesias, R.J., García-Siñeriz, J.L., Lloret, A., Huertas, F., 2020b. Physical evolution of a bentonite buffer during 18 years of heating and hydration. Eng. Geol. 264, 105408. https://doi.org/10.1016/j.enggeo.2019.105408.

Xu, L., Ye, W.M., Ye, B., Chen, B., Chen, Y.G., Cui, Y.J., 2015. Investigation on gas migration in saturated materials with low permeability. Eng. Geol. 197, 94–102.

Yoshimi, Y., Osterberg, J.O., 1963. Compression of partially saturated cohesive soils. J. Soil Mech. Found. Div. ASCE 89 1–2. SM 4.